NANO LETTERS

Letter

pubs.acs.org/NanoLett

Dielectric Scattering Patterns for Efficient Light Trapping in Thin-Film Solar Cells

Claire van Lare,[†] Frank Lenzmann,[‡] Marc A. Verschuuren,[§] and Albert Polman*,[†]

[†]Center for Nanophotonics, FOM Institute AMOLF, Science Park 104, 1098 XG Amsterdam, The Netherlands

[‡]Energy Research Center of The Netherlands, P.O. Box 1, 1755 ZG Petten, The Netherlands

[§]Philips Research Laboratories, High Tech Campus 34, 5656 AE Eindhoven, The Netherlands

ABSTRACT: We demonstrate an effective light trapping geometry for thin-film solar cells that is composed of dielectric light scattering nanocavities at the interface between the metal back contact and the semiconductor absorber layer. The geometry is based on resonant Mie scattering. It avoids the Ohmic losses found in metallic (plasmonic) nanopatterns, and the dielectric scatterers are well compatible with nearly all types of thin-film solar cells, including cells produced using high temperature processes. The external quantum efficiency of thin-film a-Si:H solar cells grown on top of a nanopatterned Al-doped ZnO, made using soft imprint lithography, is strongly enhanced in the 550−800 nm spectral band by the dielectric nanoscatterers. Numerical simulations are in good agreement with experimental data and show that resonant light scattering from both the AZO nanostructures and the embedded Si nanostructures are important. The results are generic and can be applied on nearly all thin-film solar cells.

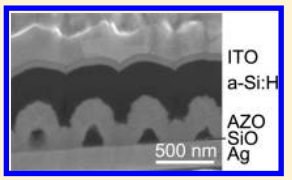

KEYWORDS: *Thin film solar cells, light trapping, resonant nanostructures, nanophotonics, geometrical resonances*

Thin-film solar cells combine the advantages of low material consumption and the possibility of mechanically flexible devices. A major problem in all thin-film solar cells is the incomplete absorption of the near-bandgap light. In order to let a device satisfy the opposing requirements of being optically thick and electrically thin, efficient light trapping is required.[1,2] Many different light trapping geometries have been studied, including randomly textured transparent conductive oxide layers, and random and periodic arrays of nanocones, nanodomes, nanorods, and nanoparticles.[3−13]

Metal nanoparticles have been studied extensively in light trapping geometries since they exhibit plasmon resonances, which leads to large scattering cross sections.[14] Recently, wavelength-sized dielectric nanoparticles have gained interest for applications in light trapping. Dielectric particles exhibit geometrical (Mie) resonances in which the light is confined inside the nanoparticle.[15] Similar to metallic nanoparticles, these particles have large scattering cross sections on resonance, exceeding their geometrical cross sections. However, a key advantage of dielectric nanoparticles is that they do not suffer from Ohmic losses that occur in metallic nanoparticles. As has been shown before, arrays of dielectric nanoparticles at the surface of a solar cell can serve to enhance the coupling of light in the cell, leading to an enhanced blue response.[16−19] The physical mechanism of this antireflection effect by nanoparticles is similar to that of light trapping, the light is coupled to a higher mode-density. However, the antireflection effect mostly depends on single-particle resonances, whereas in light trapping both the single-particle resonances and the array periodicity play an important role. Dielectric nanostructures composed of narrow cones at the rear of the cell have been studied by numerical simulations, and showed enhanced light trapping.[20]

So far, the use of engineered dielectric scattering patterns at the rear side of a thin-film solar cell has not been studied experimentally. Backscattering structures in thin-film solar cells are required to couple the poorly absorbed red and near-infrared light to waveguide modes of the thin active layer.[13,21−23] The blue light does not interact with these structures as it is absorbed in the top of the device. To simultaneously optimize the red- and blue response front- and back patterning could be combined.[24] Typical backscattering backreflectors are composed of corrugated metallic nanostructures.[25−28] In these geometries the light trapping efficiency is limited by Ohmic dissipation in the metal by the generation of localized surface plasmons and surface plasmon polaritons. Here, we experimentally and numerically study dielectric backscattering patterns integrated at the interface between a flat metallic back contact and the active layer of the cell. Using soft-imprint lithography, we fabricate SiO nanoparticles on a flat Ag back contact that is first deposited on a glass substrate, followed by overcoating with aluminum-doped zincoxide (AZO), an hydrogenated amorphous Si (a-Si:H) active layer (consisting of p-doped, intrinsic, and n-doped a-Si:H), and an indium−tin-oxide (ITO) transparent front contact. Figure 1a shows the geometry, together with the "conventional" nanostructured metallic back contact.[25−28] The AZO layer is present in all cell types, since it acts as a buffer layer to prevent diffusion of the metal into the absorber layer. For reference, measurements were also made on flat cells and conventional thin-film a-Si:H cell geometry, with a Ag/AZO/a-Si:H/ITO layer stack grown onto an Asahi U-type textured glass substrate. In the

Received: November 27, 2014
Revised: June 18, 2015

DOI: 10.1021/nl5045583
Nano Lett. XXXX, XXX, XXX−XXX

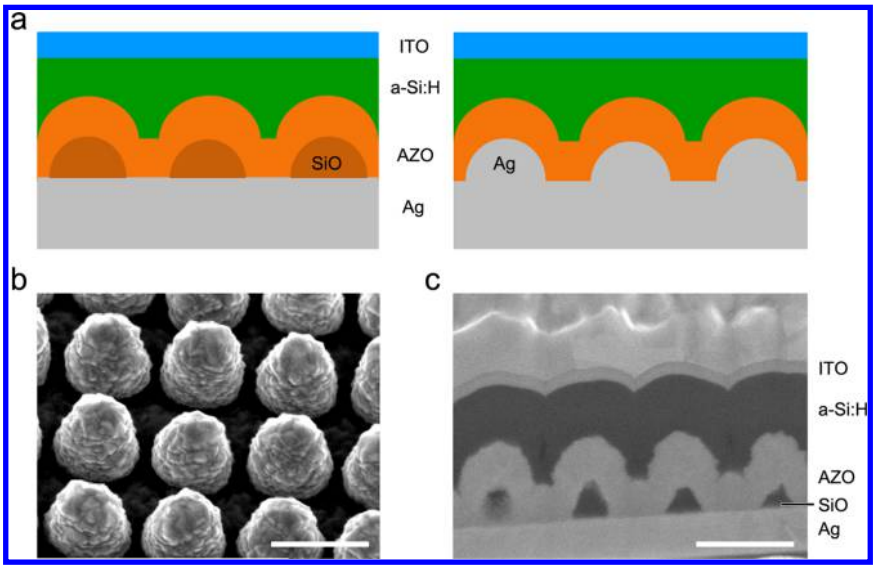

Figure 1. (a) Schematic of the studied dielectric backpattern geometry, together with the "conventional" nanostructured metallic backpattern. (b) Top-view SEM image (angle: 30) of AZO scattering pattern (thickness 300 nm) deposited onto SiO_2 nanoparticles. (c) Cross section of the full device made using FIB milling. Scale bars: 500 nm.

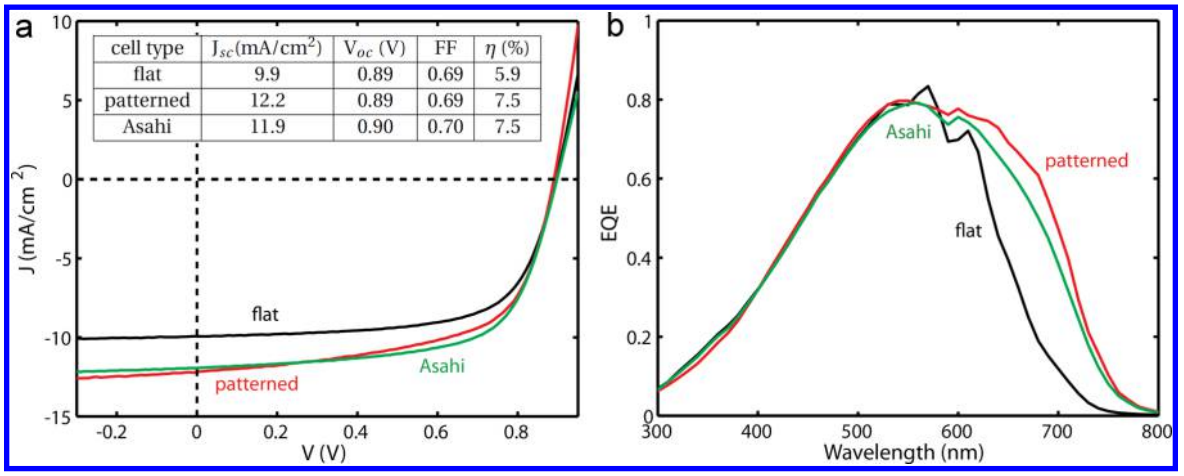

Figure 2. (a) Current−voltage characteristics for cells with flat back contact (black), periodic dielectric back pattern (red), and Asahi-nanopatterned metallic back contact (green). The inset shows the measured cell parameters for each type. (b) External quantum efficiency spectra for the same cells.

schematic drawing in Figure 1a we left out the small amount of corrugation at the top surface, since the roughness left at the top is only small. External quantum efficiency measurements shown in this paper demonstrate no antireflection effect caused by the corrugation at the front interface.

We demonstrate, both experimentally and through numerical simulations, that resonant light scattering from the dielectric nanostructures integrated between the active layer and the flat metal contact leads to enhanced light trapping, more efficient than nanostructured metallic back contacts. The dielectric nanoparticles used in this geometry are very compatible with nearly all types of thin-film solar cells, including cells that require high-temperature processing, such as $Cu(In,Ga)Se_2$, whereas integration of plasmonic particles is challenging in high-temperature cell processes due to diffusion of the metals into the absorber layer.[29] Furthermore, the dielectric light scattering insights presented here are generic, and can be applied to nearly all thin-film geometries, provided that the ingredients, like the AZO layer and the highly reflective Ag layer are compatible with the cell process. The enhanced light trapping results in increased solar energy conversion efficiencies and can be used to reduce the active layer thickness, leading to lower fabrication costs while maintaining high efficiencies.

Figure 1b shows a scanning electron microscopy (SEM) image of the dielectric scattering pattern, consisting of a periodic array of AZO scatterers, fabricated using substrate conformal imprint lithography (SCIL). A cross section of the completed device, made using focused ion-beam milling, is shown in Figure 1c. The refractive index contrast between the SiO particles and the AZO is very small; n = 1.7 for SiO and n = 1.9 for AZO.

Results. Figure 2a shows current−voltage measurements for the dielectric nanopatterned cell (red), as well as for the Asahi (green) and flat (black) reference cells. As can be seen, all three types show similar open circuit voltage (V_{oc} = 890−900 mV). The patterned cell shows only a slight reduction in fill factor compared to the other cells, indicating that the tall AZO particles do not significantly deteriorate the electrical quality of

DOI: 10.1021/nl5045583
Nano Lett. XXXX, XXX, XXX−XXX

the device. Figure 2b shows the external quantum efficiency (EQE) measurements on the same cells as in Figure 2a. All three types of cells show a similar blue response, indicating that small roughness at the front side of the device, caused by conformal growth, does not affect light absorption in the blue. Thinner cells did show an antireflection effect caused by the corrugation,[28] but the deposition of the 350 nm thick absorber layer has led to flattening of the corrugation at the front interface. At wavelengths above 570 nm the EQE of the flat cell (black) decreases rapidly due to poor absorption of these wavelengths in the thin absorber layers. The Asahi cell (green) shows a significant enhancement in this spectral region, due to light trapping. The cell with purely dielectric periodic scattering patterns (red) shows a red response that is substantially higher than that for the Asahi cell. Patterning the cell using dielectric scatterers results in a current generated in the 600−800 nm spectral range of 5.3 mA/cm^2, compared to 2.9 mA/cm^2 and 4.8 mA/cm^2 for the flat and Asahi cells, respectively. In our previous work on the same cell type and thickness with plasmonic patterns[13] we found that Ag nanoparticles on top of the cell enhanced the current in the 600−800 nm spectral range from 2.9 mA/cm^2 to 4.3 mA/cm^2. The enhancement obtained with the dielectric back scattering pattern is substantially larger than for the previously studied plasmonic front pattern. This demonstrates thus that cells with dielectric light scattering patterns on a flat metal back contact shows efficient light trapping in the infrared.

Three-dimensional finite-difference-in-time-domain (FDTD) simulations were performed to study the light trapping in more detail. Figure 3a shows the simulated spectra of light absorption in the active layer of the dielectrically patterned (red) and flat (black) cells. Similar to the EQE measurements, the simulation shows a substantial absorption enhancement for the patterned cell compared to the flat cell. Additionally, the simulation shows sharp peaks in the absorption of the patterned cell at wavelengths between 650 and 750 nm. These peaks are not a simulation artifact and are independent of mesh size and number of perfectly matched layers (PMLs) at the boundaries of the simulation volume. We find that the wavelength of these peaks depend on the array pitch and attribute them to waveguide mode coupling, which occurs at wavelengths where the parallel momentum provided by the periodic array matches the wavevector of one of the waveguide modes.[23,30,31] The fact that these sharp peaks are not observed in the EQE measurements is attributed to the fact that a 10 nm bandwidth was used in the measurement. Since the trends observed in the simulations are in good agreement with the experiments, simulations can be used to study geometries to which small modifications are made as well. Figure 3a also shows the simulated absorption spectra for cells with a thinner (200 nm) AZO layer (purple). In this case a further enhanced red response is observed. In previous experiments we found that varying the AZO layer thickness from 80−500 nm does not significantly affect the FF and V_{oc} of the cells.[30]

Next, we compare the light trapping in the dielectric nanopatterns with previously studied metallic nanopatterned back contacts.[28,32] Figure 3b shows the simulated spectrum of light absorption in the a-Si:H layer for a previously used Ag nanoparticle shape, composed of a hemiellipsoid with an optimized diameter of 300 nm and a height of 100 nm. The data for the geometry with a dielectric SiO particle from Figure 3a are repeated in the figure. For reference, data are also shown for a geometry with a Ag cylinder of the same diameter

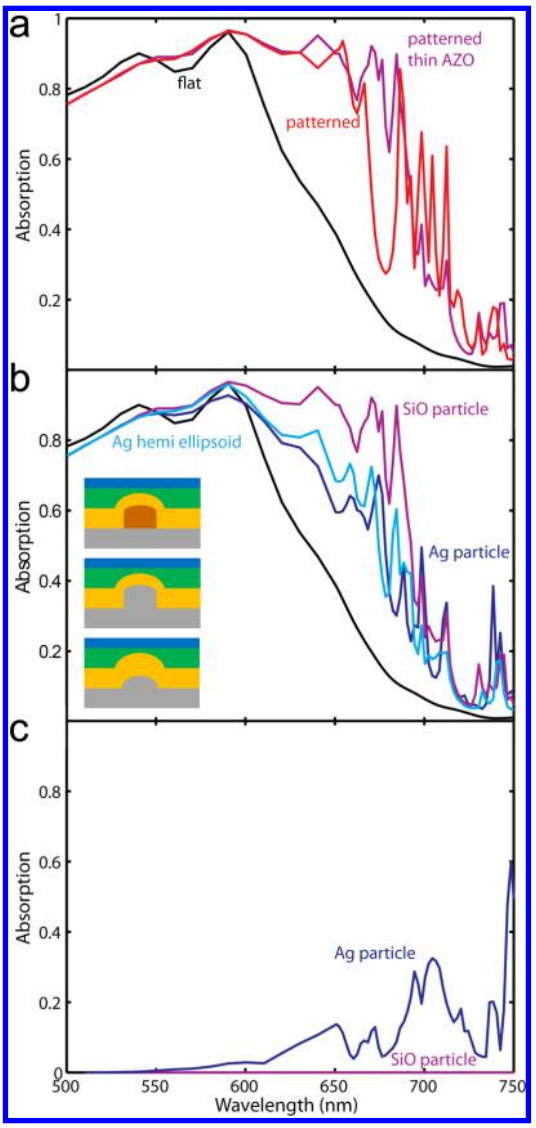

Figure 3. FDTD simulations of light absorption. (a) Absorption in a-Si:H layer for flat cell (black), periodic dielectric scattering pattern as in the experiment of Figures 1 and 2 (red) and for geometries with a thinner AZO layer (200 nm, purple). (b) Absorption in a-Si:H layer for a flat cell (black), periodic dielectric scattering pattern (purple; same data as in (a), and metallic scattering pattern with Ag hemispheres (cyan) and cylinders (blue). The inset shows a schematic of the geometries. (c) Simulated absorption in the nanoparticle for the geometries with SiO cylinders (purple) and Ag cylinders (blue).

replacing the SiO particle. In the simulations these Ag particles were covered with a patterned AZO layer such to create the same AZO outer boundaries as in Figure 3a. Note that in an experimental configuration where the AZO is conformally grown on top of the Ag particles the height of the AZO particle is determined by the height of the Ag particle. As can be seen, the metallic nanopattern performs significantly worse than the purely dielectric scattering pattern. This trend is different from the trend observed in simulations by Ferry at al.;[32] there the Ag particle array is optimized (similar to the size shown here) to maximize light trapping, and the AZO array geometry is solely determined by the Ag geometry and including conformal growth. This resulted in the use of AZO particles that are much smaller than the size required to have geometrical resonances and hence efficient scattering by the dielectric particles. In the

DOI: 10.1021/nl5045583
Nano Lett. XXXX, XXX, XXX−XXX

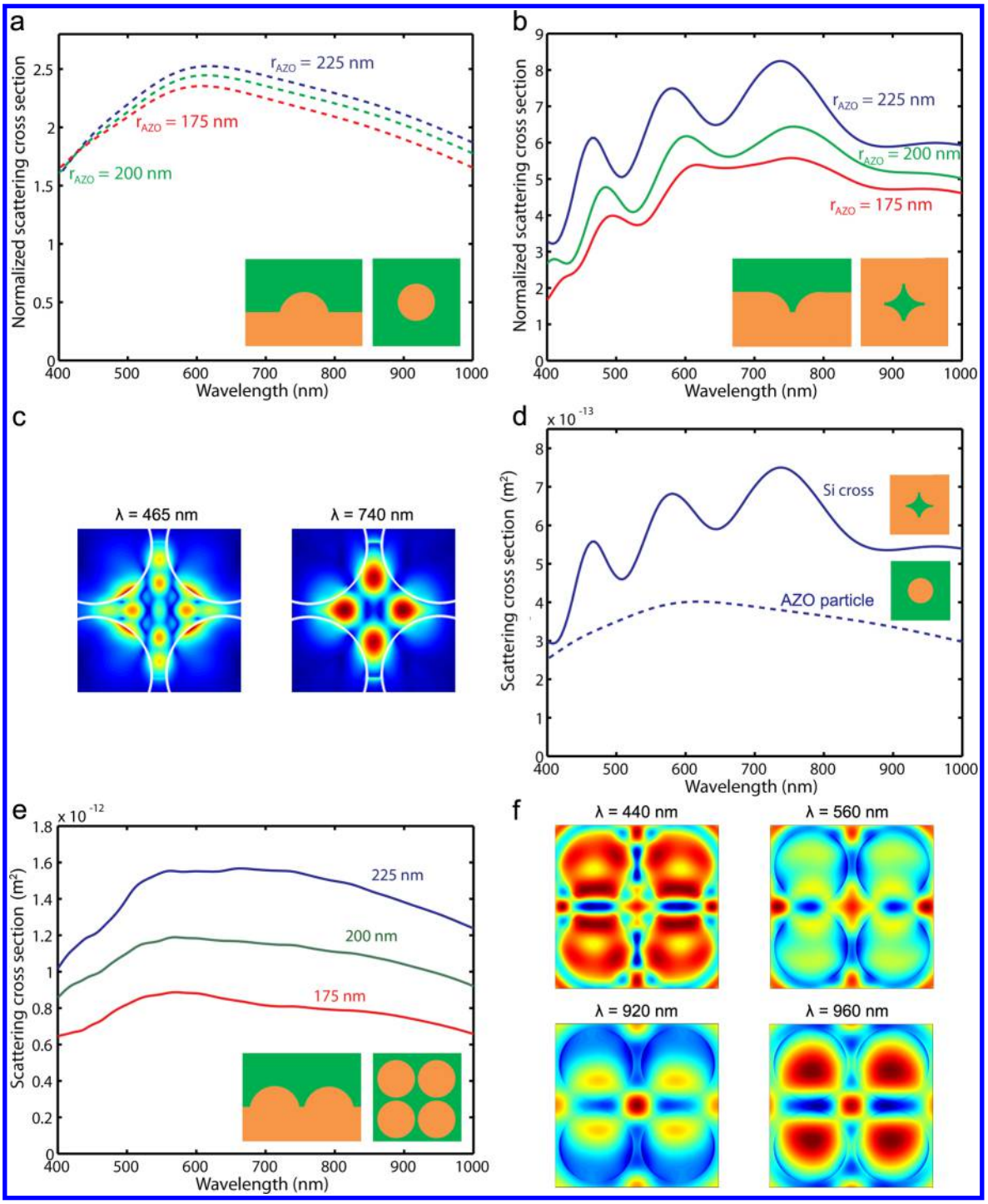

Figure 4. Simulated normalized scattering cross section of (a) single AZO particles at the AZO a-Si:H interface with radius 175 nm (red), 200 nm (green), and 225 nm (blue) and (b) single Si cross enclosed by AZO extended into the PML boundaries in a square array geometry with 500 nm pitch. Insets in (a) and (b) show left: schematic *xz*-view, right: schematic top view. (c) *XY* cross sections of the electric field intensity at two resonant peaks in (b) for the 225 nm radius AZO geometries: 465 nm (left) and 740 nm (right). The white circles indicate the positions of the AZO particles. (d) Absolute scattering cross section for the Si cross (continuous) and AZO particle (dashed). (e) Scattering cross sections for a geometry consisting of four AZO particles and one Si cross, for three different AZO particle radii. Left inset: schematic *xz*-view, right inset: schematic top view. (f) *XY*-cross sections of the electric field intensity at wavelengths of 440, 560, 920, and 960 nm.

present work the AZO particles are significantly larger than in the paper by Ferry et al.,[32] which also reduces the spacing between the particles; this is an important parameter determining efficient scattering as we will show further on. To make a fair comparison with an optimized plasmonic geometry, we use the same Ag particle size as in the work by Ferry et al. Using the optimized Ag particle size, we show that if the AZO array geometry is optimized the Ag particle is not required for light trapping and leads to additional losses by Ohmic dissipation. Data for the flat cell and the dielectrically patterned cells from Figure 3a are repeated in Figure 3b. Figure 3c shows the simulated absorption in the nanoparticle in the

DOI: 10.1021/nl5045583
Nano Lett. XXXX, XXX, XXX−XXX

geometry with a SiO cylinder (purple) and Ag cylinder (blue). As can be seen, absorption in the SiO particle is negligible, while absorption in the Ag particle is significant, in particular in the wavelengths range above 570 nm. The absorption losses in the 600−700 nm spectral range, in which the a-Si absorption still peaks to 90% of the incident light for the dielectric scattering geometry, are up to 30% in the Ag particle. This shows that, regardless of the scattering and field enhancement by the metal particles, the plasmonic geometry is too lossy to outperform the low-loss dielectric geometry. Whereas wavelength-sized metallic and dielectric nanoparticles can have comparable scattering cross sections, metal nanoparticles have substantially higher absorption cross sections than low-index dielectric materials.[33] This explains why in this spectral range the purely dielectric scattering pattern outperforms the geometry with patterned metal. Finally we note that we expect an experimental comparison between the purely dielectric scattering geometry and the geometry with patterned Ag to give similar trends in photocurrent to the trends in optical absorption shown. Because the AZO particle shapes are equal in both geometries both geometries are expected to have similar FF and V_{oc}. Therefore, in terms of overall cell efficiency we predict that the dielectric geometry will outperform the plasmonic geometry. A con of the dielectric light scattering pattern is that it will not work well on cells made of low-refractive index materials such as polymers because of the low index contrast.

To understand the physical mechanism of light scattering from the dielectric nanopatterns we simulate the scattering cross section for a single scatterer at the AZO/a-Si:H interface. Figure 4a shows the normalized scattering cross section, defined as the scattering cross section normalized to the geometrical cross section, for AZO hemiellipsoids with a height of 200 nm and radii of 175, 200, and 225 nm. Large spectral widths are observed which we attribute to radiation losses into the AZO and a-Si:H layers. The normalized scattering cross section is larger than 1 over the full 400−1000 nm spectral range indicating strong interaction with the incident light. For increasing particle radius the peak shifts to slightly larger wavelengths, consistent with the resonant (Mie) nature of the scatterer.

For the larger simulated particles, the particle diameter is close to the array pitch (500 nm). This causes the AZO particles to enclose a "Si cross" which potentially also acts as a resonant scatter. To investigate this, Figure 4b shows the normalized scattering cross section for a single Si cross enclosed by four AZO particles for AZO particle radii of 175, 200, and 225 nm and a constant array pitch of 500 nm. A smaller AZO particle radius thus corresponds to a larger Si cross. To exclude the contribution of the AZO particles to the scattering cross section, the AZO particles are connected at the point of minimum spacing between them and then extended into the PML boundaries of the simulation volume (see schematic in Figure 4b). Note that the sharp corners present in the simulated geometry would lead to poor absorber layer quality.[34,35] However, simulating this geometry allows us to understand the physical mechanism of the scattering by studying the scattering cross section of a single Si cross without having contributions from AZO particles. In the experimental configuration, the particles are not connected, and hence the sharp corners are not present. The normalized scattering cross section shows three distinct peaks. The peaks redshift with decreasing radius of the AZO particle corresponding to increasing size of the Si cross, which is consistent with a geometrical resonance in the Si cross. Figure 4c shows *xy*-cross sections of the electric field intensity 1 nm above the interface between the AZO substrate and the a-Si:H layer for the geometry with r = 225 nm. The field distributions correspond to the peaks in the scattering spectrum at 465 and 740 nm. They both show that the field is resonantly confined in the Si cross, further confirming the presence of geometrical resonances inside the Si cross.

To compare the relative contributions of the Si cross and the AZO hemiellipsoid to the total scattering in the array geometry, absolute scattering cross sections must be compared. Figure 4d compares the absolute scattering cross section for the AZO particle and the Si cross for an array geometry with 500 nm pitch and 225 nm AZO particle radius. Both scatterers have scattering cross sections in the same order of magnitude, but the scattering cross section of the Si cross (continuous line) exceeds that for the AZO particle (dashed line) over the entire spectral range. This indicates that both resonant scattering by the AZO particles and the Si crosses will play an important role in the light trapping process.

In the geometry of Figure 4d, we extended the AZO scatterers into the PML boundaries, so that the only object that could resonantly scatter the light was the Si cross. Figure 4e shows the scattering cross section for a geometry in which the Si cross as well as four finite-size AZO particles are present. In the simulations PMLs were used at all boundaries. The scattering cross section shows no distinct peaks. Figure 4f shows cross sections of the electric field 1 nm above the a-Si:H/AZO interface for four different wavelengths for the geometry with AZO particles with r = 225 nm. Complex field distributions are observed and, depending on the wavelength, the field is enhanced inside the nanoparticles or inside the Si cross. This further confirms that both types of resonant scatterers contribute to the light trapping process. The coupling to the in-plane waveguide modes will depend on the scattering cross section of the single particles, the array configuration,[36] and the coupling strength to the waveguide-modes supported by the thin-film stack.[23]

Conclusion. Dielectric light scattering patterns integrated at the interface between the active semiconductor layer and the metallic back contact of thin-films solar cells cause efficient light trapping in the red/infrared spectral band. Light is resonantly scattered into the active layer though the excitation of Mie resonances in the dielectric nanocavities. External quantum efficiency measurements on nanopatterned AZO/a-Si:H solar cells show enhanced light trapping and outperform reference cells grown on Asahi-U type texture. Numerical simulations are in good agreement with EQE measurements and show that the purely dielectric scattering pattern outperforms a combined metal−dielectric scattering pattern used in earlier work. The dielectric geometry avoids the Ohmic dissipation losses found in metallic nanopatterns. In contrast to plasmonic light trapping patterns, the dielectric scattering pattern presented here is well compatible with practically all types of thin-film solar cells, including types grown in high-temperature processes. Furthermore, the insights in light trapping presented in this paper are generic and can be applied to nearly all thin-film solar cells.

Methods. *Sample Fabrication.* Flat glass substrates were sputter-coated with 600 nm Ag, followed by 20 nm AZO, to protect the Ag back contact during fabrication of the nanoparticles. Substrate conformal imprint lithography (SCIL) was used to make the nanoparticle array, since it

DOI: 10.1021/nl5045583
Nano Lett. XXXX, XXX, XXX−XXX

facilitates high-fidelity, large-area patterning. A bilayer PDMS stamp was first molded from a master pattern that was made in a silicon wafer using electron-beam lithography. The glass/Ag/AZO stack was first spin-coated with a 500 nm PMMA layer followed by a 70 nm thick silica sol−gel layer. The SCIL stamp was then applied into the sol−gel to form a periodic array of holes in the sol−gel. Reactive ion etching was used to transfer the holes to the PMMA layer. Subsequently, a 200 nm thick SiO layer was thermally evaporated onto the samples. The PMMA/sol−gel mask was then removed by dissolving the PMMA layer in acetone. Next, the array of SiO particles was conformally coated by a 200 or 300 nm thick AZO layer by sputter deposition, leading to a periodically patterned AZO back contact. On top of the patterned AZO layer, the a-Si:H layer (350 nm i-layer) was then grown in an n−i−p configuration using plasma-enhanced chemical vapor deposition as described by Soppe et al.[37] To define electrically isolated solar cells, 4×4 mm^2 pads of ITO were sputtered on top of the a-Si:H layer using a contact mask. Finally U-shaped Ag contacts were sputtered on top through a contact mask. In parallel, reference samples without nanoparticles were fabricated on flat glass and Asahi-U type glass; depositions of the Ag, AZO, a-Si:H, and ITO layers on these samples were done in the same runs as the periodically patterned samples.

Device Characterization. *I*−*V* curves were measured under one-sun illumination using a WACOM solar simulator. EQE measurements were performed on a commercial spectral response setup (Optosolar SR300) using a 250 W xenon lamp equipped with a monochromator (Jobin Yvon iHR320). The setup was calibrated with a crystalline silicon reference solar cell, and the measurements were carried out with a spectral resolution of 10 nm. Current densities were normalized by the values obtained from external quantum efficiency (EQE) measurements to exclude inaccuracies in the determination of the surface area.

Numerical Simulations. Simulations of the light intensity inside the nanopatterned structures were carried out using Lumerical FDTD software.[38] Optical constants for the a-Si:H and ITO layers were extracted from reflection and transmission measurements on thin films on glass on materials deposited using the same deposition equipment and parameters, and optical constants for AZO and Ag were taken from literature.[39] The full thin-film stack was simulated in a unit cell with a single dielectric nanoparticle, using periodic boundary conditions in x and y directions. Perfectly matched layers were used at the top and bottom of the simulation box to absorb the light leaving the simulation volume. A mesh size of 5 nm was used for the entire layer stack. Convergence tests were done for mesh size and number of PMLs.

Scattering cross sections for a single scatterer at a AZO/a-Si:H interface were determined using refractive indices of the a-Si:H layer and the AZO layer of $n = 4.0$ and $n = 2.0$ respectively, with no imaginary parts. In this case, the a-Si:H and AZO layers were made infinitely thick by extending them into the PMLs.

AUTHOR INFORMATION

Corresponding Author

*E-mail: polman@amolf.nl.

Notes

The authors declare no competing financial interest.

ACKNOWLEDGMENTS

This work is part of the research program of FOM, which is financially supported by NWO. It is also funded by the European Research Council and NanoNextNL, a technology program of the Dutch Ministry of Economy Affairs. We thank Maarten Dorenkamper and Klaas Bakker (ECN) for the solar cell fabrication and support with the EQE measurements. SARA Computing and Networking Services is acknowledged for support in using the Lisa Compute Cluster.

REFERENCES

(1) Green, M. A. *Prog. Photovoltaics Res. Appl.* **2002**, *10*, 235−241.
(2) Yablonovitch, E.; Cody, G. D. *IEEE Trans. Electron. Dev.* **1982**, *29*, 300−305.
(3) Basch, A.; Beck, F. J.; Soderstrom, T.; Varlamov, S.; Catchpole, K. R. *Appl. Phys. Lett.* **2012**, *100*, 243903.
(4) Zhu, J.; Hsu, C.-M.; Yu, Z.; Fan, S.; Cui, Y. *Nano Lett.* **2010**, *10*, 1979−1984.
(5) Battaglia, C.; Escarré, J.; Söderström, K.; Charrière, M.; Despeisse, M.; Haug, F. J.; Baliff, C. *Nat. Phot.* **2011**, *5*, 535−538.
(6) Pala, R. A.; Liu, J. S. Q.; Barnard, E. S.; Askarov, D.; Garnett, E. C.; Fan, S.; Brongersma, M. L. *Nat. Commun.* **2013**, *4*, 2095.
(7) Soldera, M.; Estrada, E.; Taretto, K. Geometric Light Trapping in 2D and 3D Structured Small Molecule Organic Solar Cells. Symposium E/H Photovoltaic sTechnologies, Devices and Systems Based on Inorganic Materials, Small Organic Molecules and Hybrids, 2013.
(8) Yu, K. J.; Gao, L.; Park, J. S.; Lee, Y. R.; Corcoran, C. J.; Nuzzo, R. G.; Chanda, D.; Rogers, J. A. *Adv. Energy Mater.* **2013**, *3*, 1401−1406.
(9) Battaglia, C.; Söderström, K.; Escarré, J.; Haug, F.-J.; Domine, D.; Cuony, P.; Boccard, M.; Bugnon, G.; Denizot, C.; Despeisse, M.; Feltrin, A.; Ballif, C. *Appl. Phys. Lett.* **2010**, *96*, 213504.
(10) Isabella, O.; Campa, A.; Heijna, M. C. R.; Soppe, W.; Erven, R. V.; Franken, R. H.; Borg, H.; Zeman, M. Diffraction Gratings for Light Trapping in Thin-Film Silicon Solar Cells. Proceedings of the 23rd European Photovoltaic Solar Energy Conference. Valencia, Spain, 2008; pp 2320−2324.
(11) Tan, H.; Santbergen, R.; Smets, A. H. M.; Zeman, M. *Nano Lett.* **2012**, *8*, 4070−4076.
(12) Rockstuhl, C.; Fahr, S.; Bittkau, K.; Beckers, T.; Carius, R.; Haug, F.-J.; Söderström, T.; Ballif, C.; Lederer, F. *Opt. Express* **2010**, *18*, A335−A342.
(13) van Lare, M.; Lenzmann, F.; Verschuuren, M. A.; Polman, A. *Appl. Phys. Lett.* **2012**, *101*, 221110.
(14) Atwater, H. A.; Polman, A. *Nat. Mater.* **2010**, *9*, 205−213.
(15) Bohren, C. F.; Huffman, D. R. *Absorption and Scattering of Light by Small Particles*; Wiley: New York, 2008.
(16) Spinelli, P.; Polman, A. *IEEE J. Photovoltaics* **2014**, *4*, 554−559.
(17) Spinelli, P.; Verschuuren, M. A.; Polman, A. *Nat. Comm.* **2012**, *3*, 692.
(18) Spinelli, P.; Macco, B.; Verschuuren, M.; Kessels, W.; Polman, A. *Appl. Phys. Lett.* **2013**, *102*, 1233902.
(19) Zhao, Y.; Chen, F.; Shen, Q.; Zhang, L. *Appl. Opt.* **2014**, *53*, 5222−5229.
(20) Nam, W.; Ji, L.; Varadan, V.; Fonash, S. *J. Appl. Phys.* **2012**, *111*, 123103.
(21) Neviere, M.; Petit, R.; Cadilhac, M. *Opt. Commun.* **1973**, *8*, 113−117.
(22) Snyder, A.; Love, J. *Optical Waveguide Theory*; Springer Science & Business Media: London, 1983.
(23) Stuart, H.; Hall, D. *Phys. Rev. Lett.* **1998**, *80*, 5663−5666.
(24) Wang, K. X.; Z. Yu, V. L.; Cui, Y.; Fan, S. *Nano Lett.* **2012**, *12*, 1616−1619.
(25) Bhattacharya, J.; Chakravarty, N.; Pattnaik, S.; Slafer, W. D.; Biswas, R.; Dalal, V. L. *Appl. Phys. Lett.* **2011**, *99*, 131114.

DOI: 10.1021/nl5045583
Nano Lett. XXXX, XXX, XXX−XXX

(26) Haug, F.-J.; Söderström, T.; Cubero, O.; Terrazzoni-Daudrix, V.; Ballif, C. *Appl. Phys.* **2008**, *104*, 064509.
(27) Paetzold, U. W.; Moulin, E.; Michaelis, D.; Böttler, W.; Wächter, C.; Hagemann, V.; Meier, M.; Carius, R.; Rau, U. *Appl. Phys. Lett.* **2011**, *99*, p181105.
(28) Ferry, V. E.; Verschuuren, M. A.; Lare, M. V.; Schropp, R. E. I.; Atwater, H. A.; Polman, A. *Nano Lett.* **2011**, *11*, 4239−4245.
(29) Schmid, M.; Klaer, J.; Klenk, R.; Topič, M.; Krč, J. *Thin Solid Films* **2013**, *527*, 308−313.
(30) van Lare, M.; Lenzmann, F.; Polman, A. *Opt. Express* **2013**, *21*, 20738.
(31) Black, R.; Gagnon, L. *Optical Waveguide Modes: Polarization, Coupling and Symmetry*; The McGraw-Hill Companies, Inc: New York, 2010.
(32) Ferry, V.; Polman, A.; Atwater, H. *ACS Nano* **2011**, *5*, 10055−10064.
(33) van Lare, M. Light trapping in thin-film solar cells using dielectric and metallic nanostructures. Ph.D. thesis; University of Amsterdam, 2014.
(34) Söderström, K.; Haug, F.-J.; Terrazoni-Daurix, V.; Nuiquille, X.; Python, M.; Baliff, C. *J. Appl. Phys.* **2008**, *104*, 104505−104505.
(35) Li, H.; Franken, R.; Rath, J.; Schropp, R. *Sol. Energy Mater. Sol. C* **2009**, *93*, 338−349.
(36) Ferry, V. E.; Verschuuren, M. A.; Li, H. B. T.; Verhagen, E.; Walters, R. J.; Schropp, R. E. I.; Atwater, H. A.; Polman, A. *Opt. Express* **2010**, *18*, A237−A245.
(37) Soppe, W. J.; Borg, H.; van Aken, B. B.; Devilee, C.; Dörenkämper, M.; Goris, M.; Heijna, M. C. R.; Löffler, J.; Peeters, P. *J. Nanosci. Nanotechnol.* **2011**, *11*, 10604−10609.
(38) Lumerical FDTD Solutions. https://www.lumerical.com/tcad-products/fdtd/.
(39) Palik, E.; Ghosh, G. *Handbook of Optical Constants of Solids*; Academic Press: New York, 1997; Vol. 3.

DOI: 10.1021/nl5045583
Nano Lett. XXXX, XXX, XXX−XXX